ChemPubSoc Europe

DOI: 10.1002/cssc.201901587

CHEMSUSCHEM Full Papers

A Crosslinked Polyethyleneglycol Solid Electrolyte Dissolving Lithium Bis(trifluoromethylsulfonyl)imide for Rechargeable Lithium Batteries

Guiying Tian,[a] Zijian Zhao,[a] Tatiana Zinkevich,[b] Katharina Elies,[c] Frieder Scheiba,*[a, b] and Helmut Ehrenberg[a, b]

Replacing liquid electrolytes with solid ones can provide advantages in safety, and all-solid-state batteries with solid electrolytes are proposed to solve the issue of the formation of lithium dendrites. In this study, a crosslinked polymer composite solid electrolyte was presented, which enabled the construction of lithium batteries with outstanding electrochemical behavior over long-term cycling. The crosslinked polymeric host was synthesized through polymerization of the terminal amines of O,O-bis(2-aminopropyl) polypropylene glycol-*block*-polyethylene glycol-*block*-polypropylene glycol and terminal epoxy groups of bisphenol A diglycidyl ether at 90 °C and provided an amorphous matrix for Li^+ dissolution. This composite solid electrolyte containing Li^+ salt and garnet filler exhibited high flexibility, which supported the formation of favorable interfaces with the active materials, and possessed enough mechanical strength to suppress the penetration of lithium dendrites. Ionic conductivities higher than 5.0×10^{-4} S cm^{-1} above 45 °C were obtained as well as a wide electrochemical stability window (>4.51 V vs. Li/Li^+) and a high Li^+ diffusion coefficient ($\approx16.6\times10^{-13}$ m^2 s^{-1}). High cycling stability (>500 cycles or 1000 h) was demonstrated.

Introduction

Conventional lithium-ion batteries utilizing liquid electrolytes with organic carbonates as solvents (e.g., LP30) have achieved commercial success in the electronics market.[1,2] However, they can be hazardous because of their flammability and low durability caused by electrolyte leakage and the formation of lithium dendrites. The replacement of liquid electrolytes with solid electrolytes is a promising way to satisfy the stringent safety requirements of the automotive industry and other safety-relevant applications.[3] Additionally, with the help of solid electrolytes, metallic lithium might be applied as an anode material. Because metallic lithium exhibits the highest specific capacity (3860 mAh g^{-1} or 2061 mAh cm^{-3}) and lowest electrochemical potential (−3.04 V vs. standard hydrogen electrode), higher energy densities could be realized.[4,5] The ideal solid electrolyte should possess a high ionic conductivity, high electrochemical/chemical stability, and a wide potential window. Furthermore, it should be easily processable and chemically compatible with the active materials and other cell components. Solid electrolytes can be categorized into three types: inorganic sulfide- and oxide-based electrolytes and organic polymer-based electrolytes. Despite having high bulk ionic conductivities, typical oxide-based solid electrolytes (super Li^+ conductors) cannot fully contact the interior electrode, resulting in low capacity and energy density.[6–8] Expensive sulfide-type electrolytes display poor chemical stability when in contact with moisture and lithium.[9] Owing to its high donor number to coordinate Li^+ ions, high dielectric constant, and strong Li^+ solvating ability, polyethylene oxide (PEO) has been intensively studied as a polymer electrolyte host. Stable PEO-Li salt electrolytes are soft enough to make good contact with electrodes or can even be directly used as a binder. However, they suffer from low ionic conductivities (10^{-5}–10^{-3} mS cm^{-1} at room temperature) because segmental mobility of semi-crystalline PEO is limited by crystalline domains.[10] If the working temperature is increased above the melting point, the molten PEO host loses its dimensional stability, leading to a short circuit. Furthermore, the PEO-based solid electrolytes cannot block the penetration of dendrites.[11] This leads to the dilemma that highly flexible polymers show improved ionic transport properties but fail in terms of rigidity.

[a] Dr. G. Tian, Z. Zhao, Dr. F. Scheiba, Prof. Dr. H. Ehrenberg
Institute for Applied Materials (IAM)
Karlsruhe Institute of Technology (KIT)
Hermann-von-Helmholtz-Platz 1, 76344 Eggenstein-Leopoldshafen (Germany)
E-mail: frieder.scheiba@kit.edu

[b] Dr. T. Zinkevich, Dr. F. Scheiba, Prof. Dr. H. Ehrenberg
Helmholtz-Institute Ulm for Electrochemical Energy Storage (HIU)
Helmholtzstrasse 11, 89081 Ulm (Germany)

[c] K. Elies
Institute for Biological Interfaces (IBG)
Karlsruhe Institute of Technology (KIT)
Engesserstraße 18, 76128 Karlsruhe (Germany)

Supporting Information and the ORCID identification number(s) for the author(s) of this article can be found under: https://doi.org/10.1002/cssc.201901587.

It has also been shown that a crosslinked polymer host can provide good interfacial contact with the electrode in solid-state batteries, especially compensating for volume variation during cycling (e.g., when using Li metal, silicon, and sulfur).[12] In addition, the crosslinked structure can reduce the tacticity of the polymer hosts, leading to low crystallinity and robust mechanical properties. Furthermore, it can also improve the structural stability above the melting point.[13–16] For example, Tao et al. prepared a physically crosslinked network [polyurethane–PEO–lithium bis(trifluoromethylsulfonyl)imide (LiTFSI)] by hydrogen bonding interactions in solid polymer electrolytes, which showed high lithium solubility and high mechanical stability.[17] Oliveira da Silva used an epoxy resin loaded with 50 wt% [DMIM]Br (DMIM = 1-decyl-3-methylimidazolium) ionic liquid and achieved an ionic conductivity $>10^{-3}$ S cm^{-1} at 50 °C.[18] Yoshima et al. used a polyacrylonitrile (PAN)-based crosslinked gel blended with $Li_7La_3Zr_2O_{12}$ (LLZ) as a hybrid electrolyte, which exhibited a conductivity of 5.97 mS cm^{-1} at 25 °C, higher than that of the PAN-based gel electrolyte.[19] Falco et al. applied a UV-light-induced crosslinking process to prepare a composite electrolyte of LLZ in a PEO/tetraglyme matrix. This electrolyte exhibited a high ionic conductivity (0.1 mS cm^{-1} at 20 °C).[20] In summary, for improved conductivity and mechanical strength, the segmental flexibility and bulk structural stability of crosslinked polymer hosts should be studied for composite solid electrolytes (CSEs). Interestingly, researchers have found that the addition of LLZ fillers into polymer electrolytes can directly enhance the mechanical strength, ionic conductivity, and Li/electrolyte interfacial compatibility. Notably, this observation is irrespective of whether linear or crosslinked polymer hosts were used.[21–24]

Similar to PEO, polyethyleneglycol is a compound of the ether-glycol type containing several ether linkages. Strong Li^+ coordination induced by oxygen atoms is found in linear glycol ethers of suitable lengths, which makes polyethyleneglycol a promising solid electrolyte host.[25] To combine efficient Li^+ motion at the microscale and enough mechanical strength at the macroscale, we prepared a crosslinked polyethyleneglycol by the polymerization of terminal active groups. The bulk structural and thermal stability can be improved by incorporating garnet fillers. We also studied the ionic conductivity, cycling stability, and ionic mobility. The results confirm that the crosslinked structure and close contact between the electrolyte and electrode are beneficial for the improvement of battery performance.

Results and Discussion

Chemical and structural characterization

In polymer solid electrolytes, Li^+ ions prefer to coordinate to four or six ether-oxygens, and Li^+ transport occurs when the initial coordination breaks and a new one forms. Like PEO, the backbone of O,O′-bis (2-aminopropyl)polypropylene glycol-*block*-polyethylene glycol-*block*-polypropylene glycol (ED600) is rich in ether-bound oxygen, which can easily coordinate Li^+ ions.[16,26] In this study, the polymerization of terminal active epoxy and amine groups of bisphenol A diglycidyl ether (BDE) and ED600, respectively, was used to produce a crosslinked host for mobile Li^+ ions. Fourier-transform (FT)IR characterization was used to obtain structural information about the organic and inorganic components. FTIR spectra of the pristine and crosslinked structures are shown in Figure 1a. In the PEO and PEO-LLZ spectra, the peaks located at 1095 and 1461 cm^{-1} correspond to the –C–O–C– stretching and –CH_2 bending of the –$(CH_2CH_2O)_n$– backbone. The absent stretching vibration and bending mode of HO– at approximately 2875 cm^{-1} of the LLZ verified that no protonation (substitution of Li by H) occurred during the storage process.[27] After the addition of LiTFSI into the PEO-LLZ, peaks at 738 and 790 cm^{-1} appeared owing to the symmetric bending and stretching modes of –CF_3 and C–S groups of the $(TFSI)^-$ anion, respectively.[14] After the crosslinking of the terminal amine groups of ED600 and terminal epoxy groups of BDE at 90 °C, a peak at 1510 cm^{-1} was observed for the crosslinked composite electrolyte containing ED600, BDE, LLZ, PEO, and lithium salt (BEPEO-LLZ), which was ascribed to the –C=C– stretching of the benzene

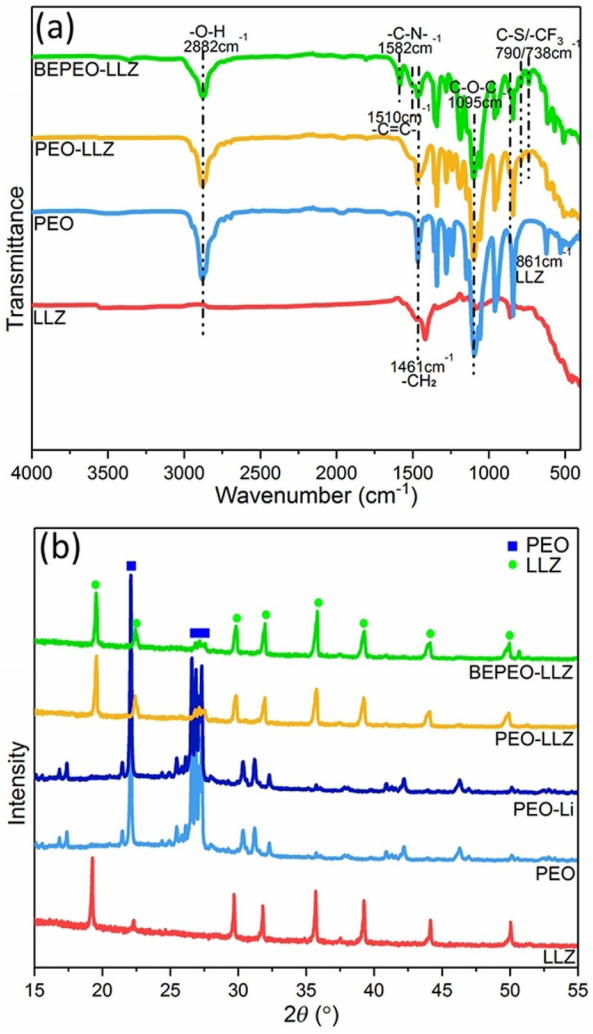

Figure 1. (a) FTIR spectra and (b) XRD patterns of the raw components and the CSE films.

rings of bisphenol A. Furthermore, a peak at 1582 cm^{-1}, corresponding to –C–N– symmetric stretching, appeared in the FTIR spectrum of the BEPEO-LLZ film, which confirmed the crosslinking of the two monomers. Gel permeation chromatography (GPC) confirmed the existence of unlinked polymer chains (M_w = 17315 and M_p = 10074) in the BEPEO-LLZ, as shown in Figure S1 in the Supporting Information. For the GPC test, BEPEO-LLZ was dispersed in dimethylacetamide (DMAC) overnight to dissolve possible unlinked polymer chains or unreacted monomers. By weighing the BEPEO-LLZ film before dissolution of soluble components in DMAC and after drying of the wet film, a mass loss of approximately 7 wt% was observed. This confirmed that most monomers in the BEPEO-LLZ film were crosslinked and a small fraction formed unlinked chains. However, no evidence was found for the presence of unreacted monomers in the film. This indicated that the polymer chains in the BEPEO-LLZ were connected by chemical crosslinking and partially by physical entangling. In addition, the strong polarity of such groups aids the dissolution of Li^+ ions in the polymer host, improving mobile carrier density.[28] In Figure 1b, the peak that was attributed to the polymer phase between 21.1 and 28.4° for the PEO-LLZ and BEPEO-LLZ samples became much weaker compared with the pure PEO and the PEO-Li films. The incorporation of LiTFSI can activate the CSE and improve its ionic conductivity,[28] but no corresponding peak was observed in the PEO-Li pattern, confirming the complete dissolution of Li salt in the polymer host.[17] Low-intensity peaks attributed to PEO were observed in both the PEO-LLZ and BEPEO-LLZ, but this information cannot be used as a criterion to estimate the crystallinity of the polymer host because it may be also ascribed to the variation of the thickness and PEO fraction of the CSE films.

The polymerization reaction used for the synthesis of the polymer host is shown in Figure 2a. The BDE contains two terminal epoxy groups and links one ED600 chain, which leads to crosslinking. As shown in the insets, the soluble sol was transformed into an immobile gel after crosslinking. As illustrated in Figure 2b, LiTFSI salt was selected as a source of Li^+ salts because the large $TFSI^-$ anions easily dissolve in the polymer host, contributing to an increased amount of free Li^+ ions.[29] As shown in Figure 3a, the fillers were homogeneously dispersed throughout the BEPEO-LLZ film. The LLZ particles had an average size of (743 ± 194) nm (see Figure S2 in the Supporting Information), as determined by SEM, whereas Rietveld refinement confirmed that the LLZ consisted of 90.3 wt% cubic phase ($Ia\bar{3}d$) and 9.7 wt% tetragonal phase ($I4_1/acd$). It has been reported that LLZ fillers can increase the carrier mobility of polymer electrolytes by enhancing the segmental motion of the polymer chains by decreasing the crystallinity of the polymer phase.[30] However, because the BEPEO-LLZ film was amorphous owing to crosslinking, the effect of the LLZ particles was considered to mainly enhance the mechanical film stability. An SEM image confirmed that there were no voids between the ceramic phase and the polymer phase. Because smooth interfaces contribute to an even current distribution during the (dis)charge processes, this should help to avoid polarization losses.[13] In contrast, voids in the PEO host and embedded filler particles were clearly dispersed on the rough surface (Figure 3b).

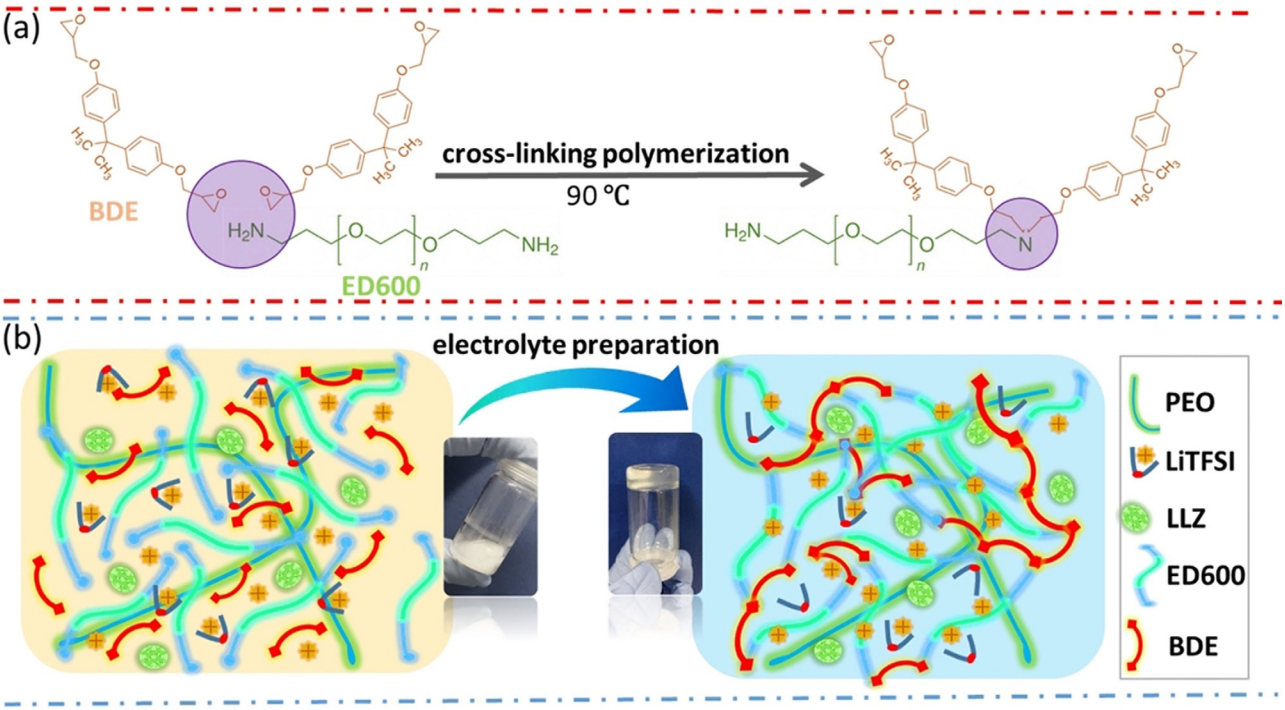

Figure 2. (a) Cross-linking illustration of ED600 and BDE; (b) schematic representation of the preparation BEPEO-LLZ CSE; photographs of the precursor sol and crosslinked gel are shown in the insets.

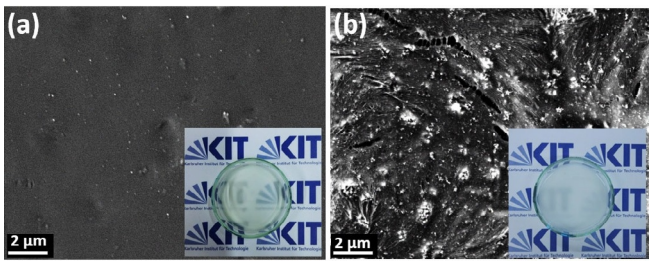

Figure 3. SEM images of (a) BEPEO-LLZ film and (b) PEO-LLZ film with corresponding photographs.

Electrochemical performance

Ion conductivity is the fundamental property of CSE materials, and electrochemical impedance spectroscopy (EIS) is a powerful technique to analyze this by an equivalent-circuit model. The obtained Nyquist plots achieved during the heating process are shown in Figure S3 in the Supporting Information. Examples of individual plots are shown in Figure 4a,b. The Nyquist plots display semicircles in the high-frequency region and oblique lines in the low-frequency region below 45 °C, but only oblique lines were observed above 45 °C. As shown in Figure 4c,d, an equivalent circuit (R_e—(R_b/CPE)—(C_{in}/R_{in})—W_a) was proposed for the data to fit the blocking electrolyte behavior, in which R_e, R_b, CPE, C_{in}, R_{in}, and W_a represent the contact resistance, the bulk resistance, the constant phase element, the double-layer capacitance at interfaces, the interface resistance, and the Warburg element, respectively.[31–33] Based on the equation $\sigma_t = l/A \times R$, in which l, A, and R represent the thickness [cm] (average of five measurements by Sylvac thickness meter), electrode area [cm^2], and total resistance [Ω] of the CSE films, respectively, temperature-dependent ionic conductivities were calculated, as depicted in Figure 4e and listed in

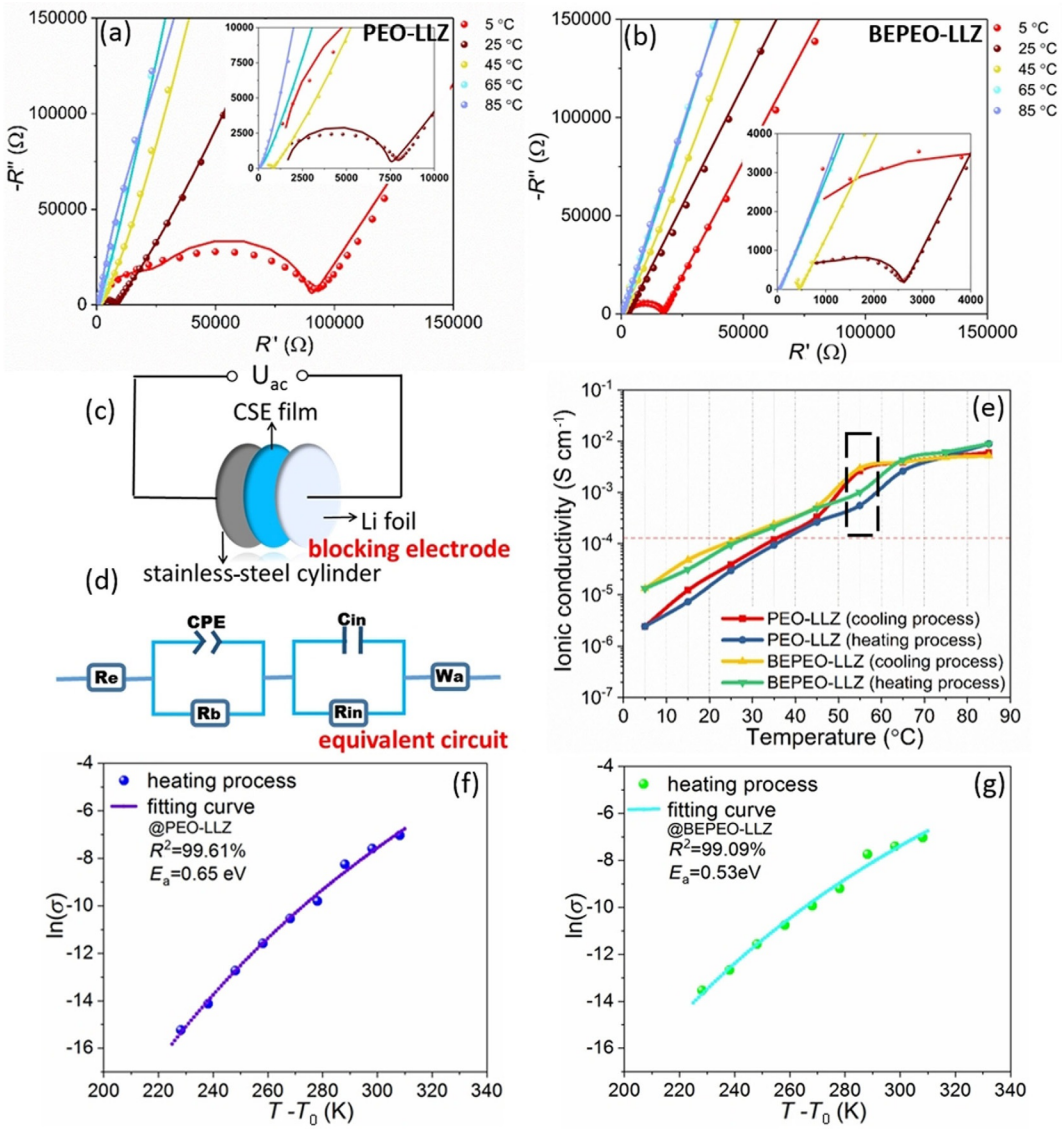

Figure 4. Selected Nyquist plots of (a) PEO-LLZ and (b) BEPEO-LLZ during heating; (c) illustration of the blocking electrode and (d) equivalent circuit used for fitting data; (e) conductivities of the PEO-LLZ and BEPEO-LLZ films during cooling and heating; temperature dependence of ln(σ) plots in the heating process and VTF fits showing the (f) PEO-LLZ and (g) BEPEO-LLZ films.

Table S2 in the Supporting Information. The ionic conductivities of the CSEs increased with temperature because the thermally activated transient mobility of the polymer chains enhanced the Li^+ mobility. In detail, BEPEO-LLZ exhibited higher ionic conductivity than PEO-LLZ below 65 °C. This confirmed that crosslinking leads to a low amount of crystalline phase, which supports the formation of a long-range pathways for Li^+ transfer. At the same testing temperature, the CSE films displayed higher conductivities during cooling than during heating. This was attributed to the thermal history and the slow recrystallization of polymer chains below the melting point.[32,34,35] At higher temperatures (≥65 °C), the linear PEO host more easily loses its dimensional stability, disturbing favorable localized pathways for Li^+ migration, as reported by Porcarelli et al.[13] The hysteresis of the ionic conductivity was observed around the melting point (approximately 65 °C, see enclosed black rectangle in Figure 4e). This was because the linear PEO host does not easily solidify during cooling compared with the crosslinked host, temporarily showing a higher ionic conductivity. In general, the crosslinked BEPEO-LLZ film displayed a higher ionic conductivity during the heating process, and its conductivity above 45 °C exceeded 5.3×10^{-4} S cm^{-1}.

The temperature dependence of the ln(σ) plots [ln(σ) vs. $T-T_0$] during heating is well-described by the Vogel–Tamman–Fulcher (VTF) empirical equation (Figure 4f,g). The following equation was proposed to describe the ionic behavior in the in CSEs above the glass transition point of polymers, gel electrolytes, organic electrolyte solutions, and ionic liquids [Eq. (1)]:[36]

$$\sigma = \sigma_0 T^{-0.5}\exp[-E_a/R(T-T_0)] \quad (1)$$

in which σ represents the total ionic conductivity, σ_0 is the pre-exponential constant related to the number of charge carriers, T_0 (Vogel temperature) is an idealized temperature corresponding to zero-configuration entropy, which is typically 10–50 K lower than the glass transition temperature of the host polymer, E_a is the activation energy, R the gas constant (8.31446 J mol^{-1} K^{-1}), and T the testing temperature [K]. The fitted activation energy (E_a) of the PEO-LLZ was 0.65 eV. In contrast, a lower E_a was obtained for the BEPEO-LLZ (0.53 eV), implying faster Li^+ migration in the crosslinked polymer matrix.

To characterize the properties of the CSE when applied in a battery, full cells were assembled by integrating PEO-LLZ and BEPEO-LLZ films with a Li anode and an $LiNi_{1/3}Co_{1/3}Mn_{1/3}O_2$ (NCM) cathode. A cross-sectional SEM image of the full cell containing a BEPEO-LLZ film with a thickness of approximately 20 μm is shown in Figure 5a (the interfaces between the lithium metal and NCM electrodes are indicated by two cyan lines). The lithium metal and NCM electrode exhibit close contact with the BEPEO-LLZ film. Energy-dispersive X-ray spectroscopy (EDX) mappings for Ni, La, C, and Zr of the cross-section are shown in Figure 5b–e. The mapping of nickel (originating from the NCM material), lanthanum, and zirconium showed that the LLZ was homogeneously distributed throughout the NCM electrode. The BEPEO-LLZ layer was only discernible as a narrow stripe in the EDX mappings. Comparison of the lanthanum map with that of nickel also confirmed the distribution of LLZ within the BEPEO layer.

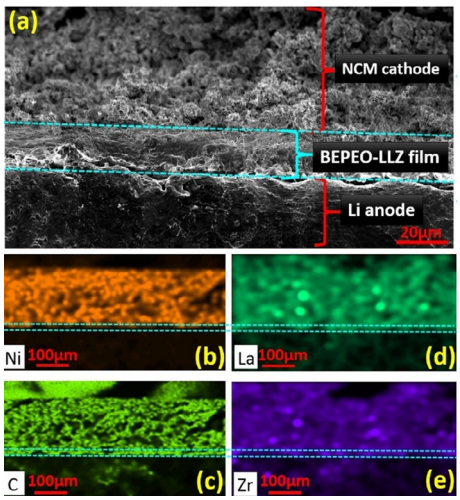

Figure 5. (a) Cross-sectional SEM images of the NCM|BEPEO-LLZ|Li electrode assembly; EDX mappings for (b) Ni, (c) C, (d) La, and (e) Zr.

To determine the electrochemical stability of the CSE film for cycling tests, linear sweep voltammetry (LSV) was performed at 45 °C measured in stainless-steel cylinder (SS)|CSE|Li cells. As shown in Figure S4a in the Supporting Information, the PEO-Li cell clearly displayed a current fluctuation from approximately 3.81 V owing to the decomposition of PEO and LiTFSI, which agreed well with the previous reports.[37,38] In contrast, the current fluctuations of the PEO-LLZ and BEPEO-LLZ commenced at approximately 4.97 and 4.51 V, respectively. The results confirmed that LLZ fillers can stabilize the polymer host and Li salt at high cell voltages.[39] However, as confirmed by the GPC result, there might be some residual terminal groups in the crosslinked BEPEO-LLZ electrolyte. The LSV result of the BEPEO-LLZ film and blends of the monomers with PEO-LLZ (Figure S4a,b in the Supporting Information) indicated that the high-voltage instability (>4.5 V) of the BEPEO-LLZ film may be caused by unreacted amine groups. Therefore, the upper potential limitation was set to 4.3 V. For galvanostatic cycling tests of the NCM electrode at 45 °C, the potential range was set to be 2.5–4.3 V vs. Li/Li^+. As depicted in Figure 6a,b, the capacities of the NCM|CSE|Li cells decreased with increasing current densities from C/25 to 1C, which is ascribed to sluggish Li^+ diffusion kinetics.[40] The PEO-LLZ-based cell exhibited a rapid drop in capacities (85, 25, 11, 2, and 91 mAh g^{-1} at C/25, C/10, C/5, C/1, and C/25, respectively), compared with the BEPEO-LLZ-based cell. The latter displayed capacities as high as 135, 109, 101, 48, and 126 mAh g^{-1} at C/25, C/10, C/5, C/1, and C/25, respectively (see Figure 6c). Capacities of the PEO-LLZ-based cell cycled at C/25 gradually decrease from approximately 105 mAh g^{-1} at the first cycle to 60 mAh g^{-1} at the 70th cycle (Figure 6d). In contrast, the BEPEO-LLZ films exhibited higher capacities (≈145 mAh g^{-1} at the initial cycle and ≈120 mAh g^{-1} at the 70th cycle). Importantly, the BEPEO-LLZ-based cell displayed a higher coulombic efficiency (≈97%) than the PEO-LLZ-based one (≈94%). This was attributed to

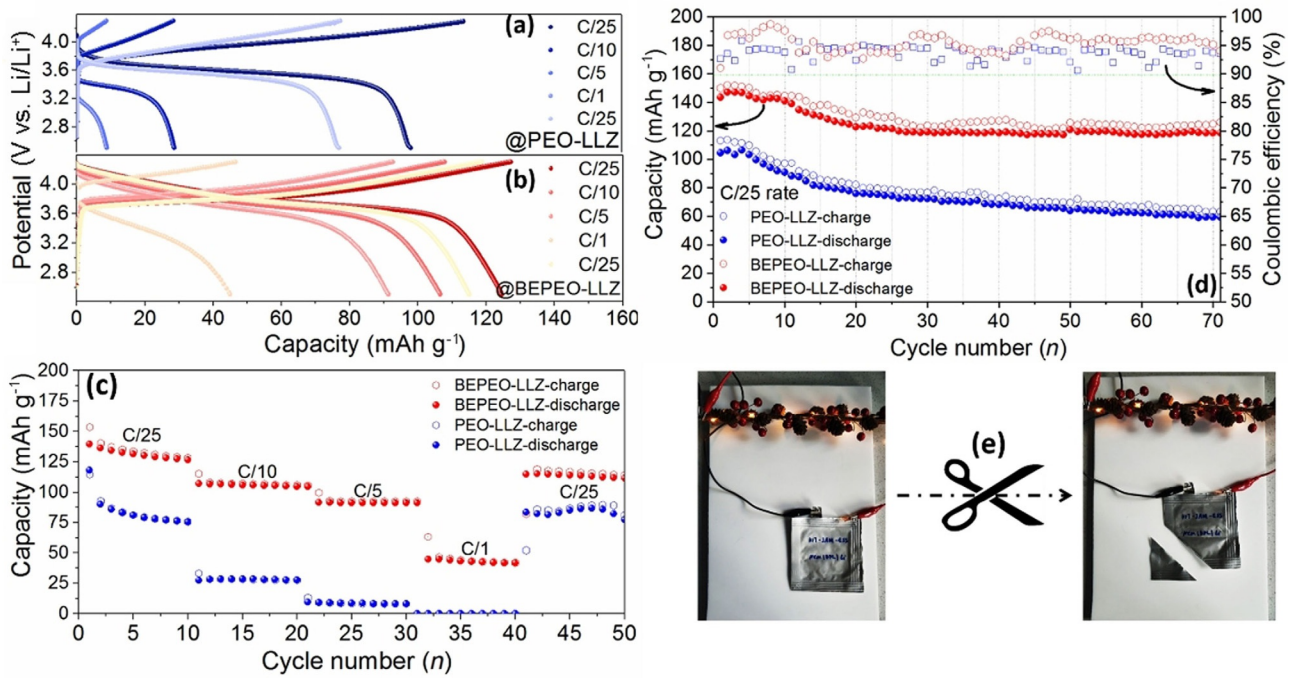

Figure 6. Fifth charge/discharge curves of the (a) NCM | PEO-LLZ | Li cell and (b) NCM | BEPEO-LLZ | Li cell cycled at C/25, C/10, C/5, C/1, and C/25, and (c) corresponding rate performance; (d) long-cycling performance (specific capacity and coulombic efficiency) of the PEO-LLZ- (blue point) and BEPEO-LLZ-based (red point) cells; (e) photographs of the pouch cell that can light up an LED light after truncation.

the improved interfacial compatibility and wettability between the BEPEO-LLZ and the electrodes.[41,42] Compared with recent reports (see Table 1), the BEPEO-LLZ-based cell in this study exhibited an acceptable capacity, especially because organic solvents were not added into the CSE as plasticizers, such as propylene carbonate (PC)[12] and tetraethylene glycol dimethyl ether (TEGDME).[41] As displayed in Figure 6e, an assembled pouch cell successfully lights up an LED light chain. When manually truncated by a ceramic knife, the pouch cell still works without short-circuiting. The electrochemical results demonstrated the practical application of a BEPEO-LLZ film for solid-state batteries.

In theory, the conductivity can be expressed as $\sigma = \Sigma n_i z_i u_i$, in which n_i is the number of free charged species, z_i is the number of charges transferred per ion, and u_i is the ion mobility. This means that the ionic conductivity depends on the active Li^+ mobility and Li^+ concentration, which is further related to Li^+ diffusion coefficient and Li^+ solubility in the amorphous part of the solid electrolyte. To elucidate the long-range diffusion and ionic mobility, pulsed-field gradient (PFG) NMR spectroscopy tests were performed on a time scale of 150 or 175 ms to record diffusion-caused damping of the signal intensity in the range of 27–70 °C. The number of repetitions was varied between 16 and 1024 scans to obtain a good signal. The obtained diffusion curves are presented in Figure 7a, b. As shown in these figures, the diffusion curve obeyed single Gaussian behavior at each temperature; thus, the single motional process was visible. Upon temperature increase, the diffusion accelerated, which is reflected in a graduate steeping of the curves. To quantify dynamical enhancement, a standard Stejskal–Tanner equation was utilized to process the data and determine the diffusion coefficient (D_{Li}). In detail, the temperature-dependent diffusion coefficients (D_{Li}) of the PEO-LLZ and BEPEO-LLZ films are displayed in Figure 7c and Table S2 in the Supporting Information.[56] The BEPEO-LLZ film exhibited a higher D_{Li} over the whole temperature range, which agreed well with the trend of ionic conductivities determined by EIS measurements (see Figure 4).

Because the electrochemical performance depends not only on the bulk conductivity of the solid electrolyte but also on the interface resistance, it is necessary to investigate the cycling and interfacial stability of the CSE films against metallic Li. Therefore, galvanostatic Li^+ stripping/plating experiments at a current density of 10 μA cm^{-2} were performed by using a symmetrical lithium metal cell. Experiments were performed at 45 °C, and a time interval of 2 h was used for a complete stripping/plating cycle. The overpotential at the 50th cycle was approximately 0.034 and 0.025 V for the PEO-LLZ and BEPEO-LLZ, respectively. In detail, severely high and fluctuating potentials were occasionally observed for the PEO-LLZ-based cell (see Figure 8a) because it suffers from polarization issues arising from uneven plating/stripping.[13] In contrast, the BEPEO-LLZ film displayed a much more stable cycling behavior, exhibiting only a slight increase in overpotential during the cycling test over 500 cycles (≥1000 h, see Figure 8c). The results indicated a good wettability of the BEPEO-LLZ film on the Li foil, which suppresses the growth of lithium dendrites during long-term cycling.[57,58] However, side reactions with the Li foil apparently led to a steady increase of the interface resistance, causing a gradual rise of the overpotential. High but mostly stable impedance of the PEO-LLZ cell was confined (Figure 8b), whereas the BEPEO-LLZ cell (Figure 8d) had a reduced resistance during

Table 1. Composition and electrochemical performance of CSE film.

Solid electrolyte	Polymerization	Conductivity	Cathode || Anode	Capacity	Ref.
TiO_2 gel, 1-ethyl-3- methylimidazolium bis(trifluoromethylsulfonyl)imide, tetrabutyl titanate with LiTFSI	esterification hydrolysis/condensation	2.8 mS cm^{-1}	$LiFePO_4$ || Li	150 mAh g^{-1} for 300 cycles at 2 C	[43]
silyl-polyether, LiTFSI, TEGDME, di-*n*-butyltin bis(2,4-pentanedionate)	polymerization	0.36 mS cm^{-1} at 25 °C	$LiFePO_4$ || Li	152 mAh g^{-1} at 0.1 C	[41]
PEO, branched acrylate; $LiClO_4$, lithium bis(oxalato)borate, LiTFSI	UV photo-polymerization	0.22 mS cm^{-1}	$LiFePO_4$ || Li	66 mAh g^{-1} at 0.5 and 5 C	[15]
PEO, TEGDME, LiTFSI	UV-light-induced polymerization	0.1 mS cm^{-1} at 25 °C	Li || TiO_2	141 mAh g^{-1} at 0.1 mA cm^{-1} at 20 °C	[13]
tripropylene glycol diacrylate and azobisisobutyronitrile in $LiPF_6$, ethylene carbonate/ethylmethyl carbonate/dimethyl carbonate	polymerization Li salt injecting	1.74 mS cm^{-1}	SiO_2/$LiFePO_4$ || Li	159.3 mAh g^{-1} and retention of 100.2 % after 200 cycles at 0.2C	[44]
poly(ethylene glycol) diacrylate, poly(ethylene glycol) diglycidyl ether, LiTFSI, benzoyl peroxide	one-pot polymerization	0.053 mS cm^{-1} at 30 °C	$LiFePO_4$ || Li	162 mAh g^{-1} at 0.2 C and 55 °C	[45]
$Li_{1.3}Al_{0.3}Ti_{1.7}(PO_4)_3$, PEO, boronized polyethylene glycol	crosslinking	2.5 mS cm^{-1} at 60 °C	$LiFePO_4$ || Li	158.2 and 94.2 mAh g^{-1} at 60 °C and 0.1 C and 2 C	[46]
montmorillonite, LiTFSI, polyvinylidenedifluoride, polyvinyl alcohol	casting method	0.43 mS cm^{-1}	$LiFePO_4$ || Li	123 mAh g^{-1} after 100 cycles at 0.1 C	[47]
poly(methacrylate), poly(ethylene glycol), $LiClO_4$, SiO_2	sonication mixing	0.26 mS cm^{-1}	$C_{35}H_{20}O_{10}$ || Li	418 mAh g^{-1}, 94.7 % capacity retention after 50 cycles at 0.2 C	[48]
poly(ethylene carbonate), lithium bis(fluorosulfonyl)imide, 3D polyimide	gel-casting	≈10^{-5} S cm^{-1} at 30 °C	$LiFePO_4$ || Li	≈125 mAh g^{-1} at 30 °C and C/20	[49]
PEO, Y-type polyether, Al_2O_3, LiTFSI	gel-casting	0.071 mS cm^{-1} at 45 °C	$LiFePO_4$ || Li	132.9 and 165.1 mAh g^{-1} at 0.2 C at 30 and 45 °C	[50]
LiTFSI, $Pyr_{14}TFSI$, $BaTiO_3$	ball-milling	1.3 mS cm^{-1} at 30 °C	$LiFePO_4$ || Li $LiCoO_2$ || Li	160 and 131 mAh g^{-1} for $LiFePO_4$ and $LiCoO_2$ at 0.1 C and 80 °C	[51]
bisphenol A ethoxylate, ethylene-oxide-based dimethacrylic oligomer, dimethyl polyethylene glycol, LiTFSI, azobisisobutyronitrile	free radical polymerization	0.14 mS cm^{-1} at 20 °C	$LiFePO_4$ || Li	120 mAh g^{-1} at 0.1 C and RT	[52]
poly(diethylene glycol carbonate), poly(triethylene glycol carbonate), substituting with triethylene glycol	gel-casting	0.011 mS cm^{-1} at 25 °C	$LiFePO_4$ || Li $LiFe_{0.2}Mn_{0.8}PO_4$ || Li	40 mAh g^{-1} at 0.1 C and 25 °C/170 mAh g^{-1} at 0.02 C and 25 °C	[53]
thermoplastic polyurethane, PEO, LiTFSI	casting	0.53 mS cm^{-1} at 60 °C	$LiFePO_4$ || Li	112 and 127 mAh g^{-1} at 1 C under 60 and 80 °C	[54]
cyanoethyl polyvinyl alcohol in polyacrylonitrile, LITFSI, $LiPF_6$	in situ polymerization	0.3 mS cm^{-1} at RT	$LiFePO_4$ || Li	N/A	[55]
poly(vinylidene fluoride-hexa-fluoropropylene), LLZ	tape-casting process	0.11 mS cm^{-1} at 25 °C	$LiFePO_4$ || Li	110 mAh g^{-1} after 180 cycles at 0.5 C	[28]
poly(propylene oxide), Jeffamine precursors, SiO_2, LiTFSI, propylene carbonate	covalent/hydrogen bonding crosslinking	0.25 mS cm^{-1} at 26 °C	$LiFePO_4$ || Li	152 mAh g^{-1} after 300 cycles	[12]
ED600, BDE, LLZ, LiTFSI, PEO	polymerization	0.53 mS cm^{-1} at 45 °C	NCM || Li	125 mAh g^{-1} after 70 cycles at 45 °C	this work

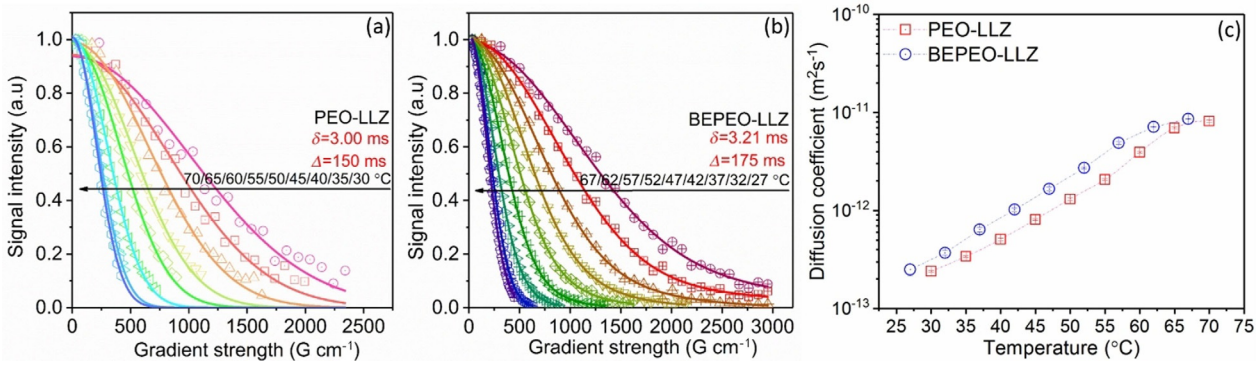

Figure 7. PFG-NMR results: echo damping versus gradient strengths of (a) PEO-LLZ and (b) BEPEO-LLZ; (c) calculated diffusion coefficient (D_{Li}).

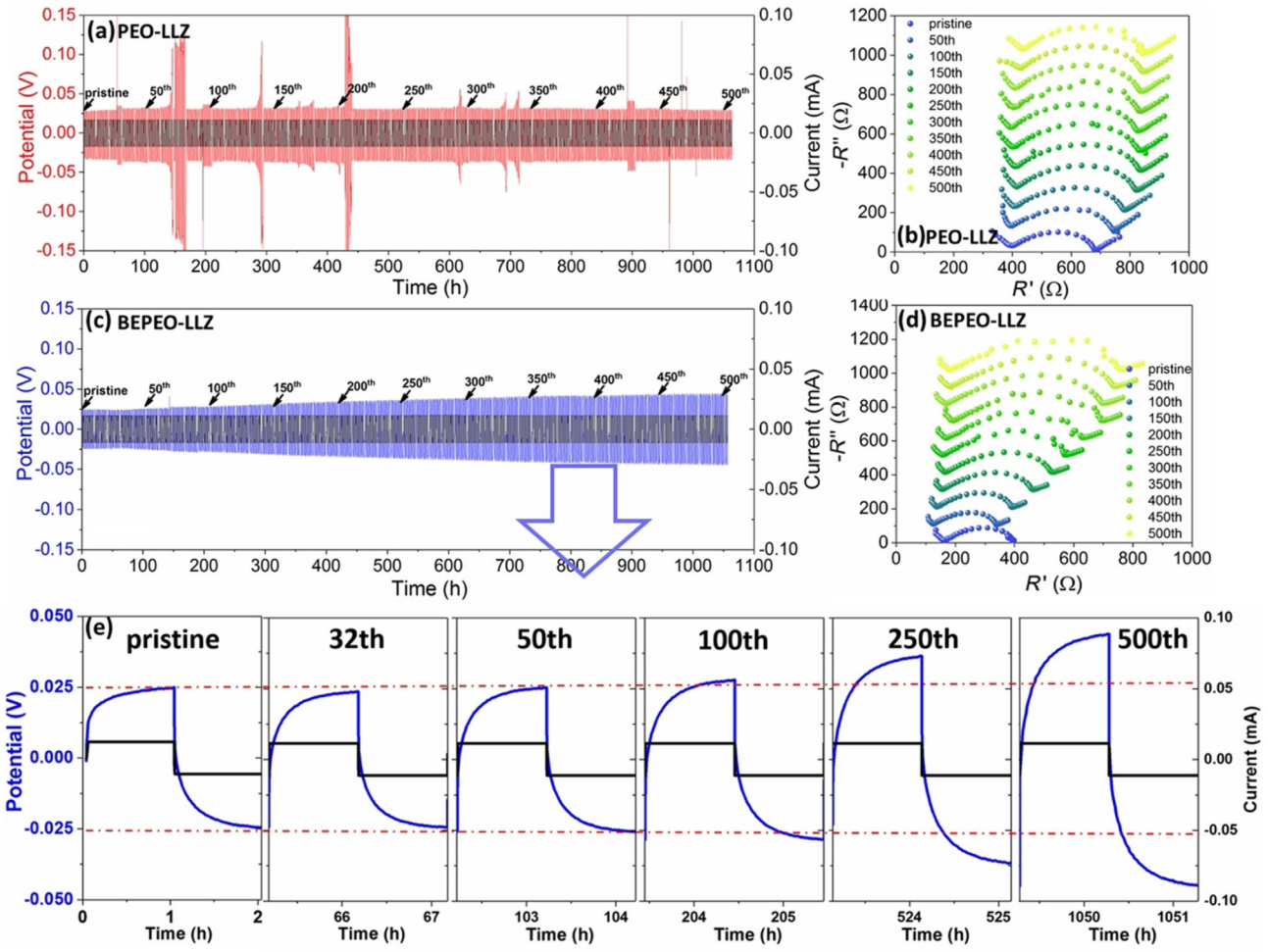

Figure 8. (a, c) Galvanostatic stripping/plating profiles and (b, d) Nyquist plots recorded every 50 cycles of PEO-LLZ and BEPEO-LLZ. Galvanostatic cycling was performed at a current density of $j = 10\ \mu A\ cm^{-2}$. (e) Selected overpotential profiles of galvanostatic cycling with the BEPEO-LLZ film.

the first 50 cycles. However, the growing solid electrolyte interphase layer led to steadily increasing interface resistances, resulting in a growing internal resistance of the cell (see Figure 7e). Therefore, despite the promising electrochemical properties of the BEPEO-LLZ electrolyte, its stability towards metallic lithium needs to be improved further.

At the melting point, the polymer completely melts, including the crystalline domains, so that the chains can move freely. This transition can be recorded by differential scanning colorimetry (DSC). In Figure 9a, the DSC curves display large endothermic peaks at approximately 75 °C for the PEO-Li and PEO-LLZ samples, whereas the BEPEO-LLZ sample has two weaker peaks at approximately 70 and 120 °C. The decrease in melting enthalpy (crystalline fraction) was evidenced by a reduced enclosed area of the endothermic peaks. The reduced crystallinity was attributed to crosslinking of the BEPEO, which impeded the formation of ordered structures of the polyethyleneglycol chains. This increases amorphicity and Li^+ transferability in the BEPEO.[59] Furthermore, thermogravimetry analysis (TGA) curves of the PEO-Li, PEO-LLZ, and BEPEO-LLZ films showed that they decompose at approximately 350 °C owing to dehydration and decomposition of the polymer host. The residual mass remained almost unchanged above 400 °C, as shown in Figure 9b. In particular, the garnet filler increased the onset of the decomposition temperature up to 348 °C for the PEO-LLZ film, compared with that of the pure PEO-Li at 329 °C and the BEPEO-LLZ at 298 °C. However, the decreased decomposition temperature is still high enough for most battery applications.

In view of the ionic conductivity, ionic mobility, cycling stability, and thermal stability, the CSE using crosslinked BEPEO-LLZ displayed excellent potential for solid-state batteries. As discussed above, the results can be attributed to three factors: 1) the crosslinked host increases the amorphous phase and Li^+ mobility; 2) the crosslinked host can stabilize favorable localized pathways at elevated temperatures; 3) long-range diffusion pathways can form along the crosslinked polymer chains owing to the Li^+ coordination process.[29]

Conclusions

An ether-rich polyethyleneglycol was synthesized by using a facile polymerization reaction and used as the amorphous host of a composite solid electrolyte. This crosslinking reaction occurred between terminal active groups [epoxy and amine

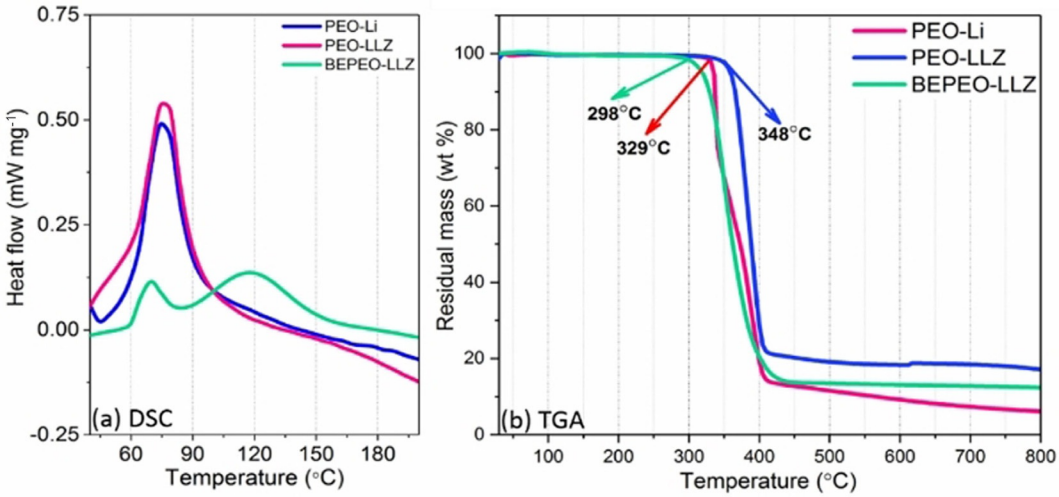

Figure 9. (a) DSC and (b) TGA curves of the CSE films under argon flow at a heating rate of 5 °C min^{-1}.

groups from O,O′-bis (2-aminopropyl)polypropylene glycol-*block*-polyethylene glycol-*block*-polypropylene glycol and bisphenol A diglycidyl ether, respectively]. The addition of $Li_7La_3Zr_2O_{12}$ (LLZ) fillers and polyethylene oxide (PEO) improved the mechanical strength and film-processing ability. This compositing strategy combines efficient ionic mobility at the microscale with increased mechanical strength at the macroscale. The as-prepared crosslinked composite electrolyte containing ED600, BDE, LLZ, PEO, and lithium salt (BEPEO-LLZ) exhibited a high ionic conductivity (5.3×10^{-4} S cm^{-1} at 45 °C), a wide electrochemical potential window (>4.51 V vs. Li/Li$^+$), and a high diffusion coefficient ($\approx16.6\times10^{-13}$ m^2 s^{-1}). Furthermore, this filler-embedded crosslinked host stayed mechanically intact above the melting point, allowing a stable operation of solid-state batteries even at elevated temperatures. The flexible host wets electrodes well, leading to a uniform current distribution at the electrode/electrolyte interface. Galvanostatic stripping/plating tests confirms a long cycle life (>500 cycles) of the BEPEO-LLZ without short-circuiting induced by lithium dendrites. These properties contribute to moderate capacities (125 mAh g^{-1} at C/25), good cycle stability, and high coulombic efficiency (>97%) of an assembled $LiNi_{1/3}Co_{1/3}Mn_{1/3}O_2$ | BEPEO-LLZ | Li solid-state cell.

Experimental Section

Preparation of composite solid electrolyte film

Commercial BDE (50 mg, liquid chromatography purity ≥95%, Sigma–Aldrich), PEO (30 mg, $M_w\approx5\times10^6$, Sigma–Aldrich), LLZ (25 mg, NEI Corporation), and LiTFSI, (EO/Li$^+$ = 8 in molar, ion chromatography purity ≥98.0%, Alfa-Aesar) were added stepwise to ED600 (Jeffamine®, 245 mg, $M_r\approx600$, Aldrich) during stirring at 1200 rpm. After degassing the polymer, sol was solidified into a quasi-solid-state gel through polymerization of terminal active groups at 90 °C for 12 h, as depicted in Figure 1a. The monomer molar ratio of ED600 and BDE was set to 1:1.5 to obtain a proper film-processing ability. The casted composite electrolyte film was abbreviated as BEPEO-LLZ. To achieve sufficient mechanical strength for film processing, small quantities of LLZ filler and macromolecular PEO were added into the BEPEO-LLZ. The incorporated LLZ was a garnet-type solid electrolyte, which was used here to improve mechanical strength and ionic conductivity.[60] As references, films consisting of PEO + LiTFSI and PEO + LiTFSI + LLZ dissolved in dimethyl carbonate (DMC, gel chromatography purity ≥99.0%, Merck KGaA) were prepared through gel-casting, abbreviated as PEO-Li and PEO-LLZ, respectively (for details of the composition see Table 2). BEPEO without LLZ fillers was too sticky to be used as a free-standing film. Thus, it is not discussed here.

General characterization

XRD was performed using Co$K_{\alpha1}$ radiation (λ = 1.78896 Å) on an STOE STADI P X-ray powder diffractometer equipped with a Mythen 1 K detector to characterize the crystalline structure of the CSEs. The surface morphology of the CSEs was investigated with a Merlin scanning electron microscope (Zeiss GmbH). TGA data were collected using an STA 449C Netzsch analyzer from 35 to 800 °C at a heating rate of 5 °C min^{-1} under an argon flow (42 mL min^{-1}). A Bruker Tensor 27 FTIR spectrometer was used to collect data from 4000–400 cm^{-1} in attenuated total reflection mode to examine the crosslinking structure. GPC was conducted using a PL-50 system equipped with a refractive index (RI) detector and three Mixed C linear columns to obtain values of mass distribution at 50 °C. The

Table 2. Detailed amounts of each component in the CSE films.

Sample	Polymer host	Li salt	Garnet filler	Preparation
PEO-Li	PEO (350 mg)	LiTFSI (50 mg)	–	gel-casting
PEO-LLZ	PEO (325 mg)	LiTFSI (50 mg)	LLZ (25 mg)	gel-casting
BEPEO-LLZ	BDE (50 mg) + ED600 (245 mg) + PEO (30 mg)	LiTFSI (50 mg)	LLZ (25 mg)	polymerization

flow rate of the testing solution was 1 mL min^{-1}, and poly(methyl methacrylate) standards were used for calibration.

PFG-NMR spectra were measured on a Bruker Avance 300 MHz spectrometer equipped with a Diff 50 probe, which produces pulsed-field gradients reaching up to 3000 G cm^{-1}. The ^{7}Li NMR spectra were measured at 116.6 MHz. A stimulated-echo pulse sequence in combination with bipolar gradients was used to observe the echo damping as a function of gradient strength. The duration of the $\pi/2$ varied from18 to 20 μs. Recycle delays in the range of 1–2.5 s were chosen on the basis of the T1 measurement results. All delay times during each PFG-NMR experiment were kept constant, whereas the gradient amplitude was varied to cause the signal decay, then the influence of relaxation on the echo decay was eliminated. The optimal values for the gradient duration (δ) and the diffusion time (Δ) were found and are indicated on the corresponding figures. In total, 16 points were acquired to form each diffusion decay.

Electrochemical evaluation

EIS tests were performed over a frequency range of 10^{6}–10^{-2} Hz with a sine amplitude of 10 mV during cooling and heating (85 °C→5 °C→85 °C). The CSE film (∅12 mm) was sandwiched by stainless-steel cylinders (SS) and assembled into a Swagelok cell. Prior to measuring, the cells were kept in a climate chamber (M53, Binder GmbH) for each temperature setting for 30 min. The obtained impedance spectra were fitted using ZsimpWin software (Ametek. Inc.). The total conductivity σ_t was calculated based on the equation $\sigma_t = l/A \times R$. The electrochemical stability window was examined in a coin cell (SS|CSE|Li) through LSV at a scanning rate of 1 mV s^{-1} at 45 °C by using SS as the blocking working electrode and lithium foil as both the counter and the reference electrode. CV was applied in a symmetrical cell (Li|CSE|Li) at a potential range of −1.0–1.0 V (vs. Li/Li^{+}) with a scanning rate of 1 mV s^{-1}. Galvanostatic cycling with Li symmetrical cells was also performed at a current density of 10 μA cm^{-2} for 2 h.

Battery tests

NCM was prepared by using a hydroxide co-precipitation method described by Hua et al.[61] A typical cathode slurry was prepared by mixing NCM powder, hybrid binder [2.5 wt% solvent [PEO/styrene butadiene rubber (SBR) = 51.6 wt%:48.4 wt%] in aqueous solution], carbon black (Super-C65, Timcal Ltd.), and LLZ at a weight ratio of 8:1:0.9:0.1. The uniform slurry was coated on an Al foil by using a laboratory coater with doctor-blade and then dried at 80 °C for 12 h. CR2032 cells were assembled in an argon-filled glovebox (MB200, MBraun GmbH) consisting of the NCM cathode foil (∅12 mm), CSE film (∅16 mm), and Li foil (∅12 mm, Alfa Aesar), then compressed under 15 MPa, and aged at 80 °C to ensure the components were closely packed. Galvanostatic charge/discharge tests were performed with a multichannel potentiostat (VMP3, Bio-Logic) with a voltage range of 2.5–4.3 V vs. Li/Li^{+}.

Acknowledgements

We acknowledge the financial support of this research by the China Scholarship Council (CSC grant no.: 201506880029/-38). The technical supports from Geckle Udo (SEM measurement) and Liuda Mereacre (TGA measurement) are also greatly acknowledged. This work contributes to the research performed at CELEST (Center for Electrochemical Energy Storage Ulm-Karlsruhe) and benefits from the BMBF funded project FESTBATT (grant no.: 03XP0176A).

Conflict of interest

The authors declare no conflict of interest.

Keywords: composite solid electrolyte · ionic conductivity · lithium batteries · polymerization

[1] G. Martin, L. Rentsch, M. Höck, M. Bertau, *Energy Storage Mater.* **2017**, *6*, 171–179.
[2] T. P. Narins, *Extr. Ind. Soc.* **2017**, *4*, 321–328.
[3] M. Yamamoto, Y. Terauchi, A. Sakuda, M. Takahashi, *Sci. Rep.* **2018**, *8*, 1212.
[4] B. Scrosati, J. Garche, *J. Power Sources* **2010**, *195*, 2419–2430.
[5] H. Kim, G. Jeong, Y.-U. Kim, J.-H. Kim, C.-M. Park, H.-J. Sohn, *Chem. Soc. Rev.* **2013**, *42*, 9011.
[6] F. Han, Y. Zhu, X. He, Y. Mo, C. Wang, *Adv. Energy Mater.* **2016**, *6*, 1501590.
[7] S. Lobe, C. Dellen, M. Finsterbusch, H.-G. Gehrke, D. Sebold, C.-L. Tsai, S. Uhlenbruck, O. Guillon, *J. Power Sources* **2016**, *307*, 684–689.
[8] Z. Zhang, Y. Shao, B. Lotsch, Y. S. Hu, H. Li, J. Janek, L. F. Nazar, C. W. Nan, J. Maier, M. Armand, L. Chen, *Energy Environ. Sci.* **2018**, *11*, 1945–1976.
[9] M. Nagao, A. Hayashi, M. Tatsumisago, T. Kanetsuku, T. Tsuda, S. Kuwabata, *Phys. Chem. Chem. Phys.* **2013**, *15*, 18600.
[10] F. Capuano, *J. Electrochem. Soc.* **1991**, *138*, 1918.
[11] H. Wang, N. Imanishi, A. Hirano, Y. Takeda, O. Yamamoto, *J. Power Sources* **2012**, *219*, 22–28.
[12] J. Lopez, Y. Sun, D. G. Mackanic, M. Lee, A. M. Foudeh, M. S. Song, Y. Cui, Z. Bao, *Adv. Mater.* **2018**, *30*, 1804142.
[13] L. Porcarelli, C. Gerbaldi, F. Bella, J. R. Nair, *Sci. Rep.* **2016**, *6*, 19892.
[14] R. Na, C. Su, Y. Su, Y. Chen, Y. Chen, G. Wang, H. Teng, *J. Mater. Chem. A* **2017**, *5*, 19703–19713.
[15] X.-X. Zeng, Y.-X. Yin, N.-W. Li, W.-C. Du, Y.-G. Guo, L.-J. Wan, *J. Am. Chem. Soc.* **2016**, *138*, 15825–15828.
[16] S.-H. Wang, S.-S. Hou, P.-L. Kuo, H. Teng, *ACS Appl. Mater. Interfaces* **2013**, *5*, 8477–8485.
[17] C. Tao, M. H. Gao, B. H. Yin, B. Li, Y. P. Huang, G. Xu, J. J. Bao, *Electrochim. Acta* **2017**, *257*, 31–39.
[18] L. C. Oliveira da Silva, B. G. Soares, *J. Appl. Polym. Sci.* **2018**, *135*, 45838.
[19] K. Yoshima, Y. Harada, N. Takami, *J. Power Sources* **2016**, *302*, 283–290.
[20] M. Falco, L. Castro, J. R. Nair, F. Bella, F. Bardé, G. Meligrana, C. Gerbaldi, *ACS Appl. Energy Mater.* **2019**, *2*, 1600–1607.
[21] J.-H. Choi, C.-H. Lee, J.-H. Yu, C.-H. Doh, S.-M. Lee, *J. Power Sources* **2015**, *274*, 458–463.
[22] C.-H. Lee, G. Park, J. Choi, C. Doh, D. Bae, J. Kim, S. Lee, *Mater. Res. Bull.* **2016**, *83*, 309–315.
[23] T. Yang, Y. Li, C. K. Chan, *J. Power Sources* **2015**, *287*, 164–169.
[24] N. M. Asl, J. Keith, C. Lim, L. Zhu, Y. Kim, *Electrochim. Acta* **2012**, *79*, 8–16.
[25] J. Mindemark, M. J. Lacey, T. Bowden, D. Brandell, *Prog. Polym. Sci.* **2018**, *81*, 114–143.
[26] B. Scrosati, F. Croce, L. Persi, *J. Electrochem. Soc.* **2000**, *147*, 1718.
[27] C. Liu, K. Rui, C. Shen, M. E. Badding, G. Zhang, Z. Wen, *J. Power Sources* **2015**, *282*, 286–293.
[28] W. Zhang, J. Nie, F. Li, Z. L. Wang, C. Sun, *Nano Energy* **2018**, *45*, 413–419.
[29] Z. Xue, D. He, X. Xie, *J. Mater. Chem. A* **2015**, *3*, 19218–19253.
[30] J. Zhang, N. Zhao, M. Zhang, Y. Li, P. K. Chu, X. Guo, Z. Di, X. Wang, H. Li, *Nano Energy* **2016**, *28*, 447–454.
[31] J. Zheng, M. Tang, Y.-Y. Hu, *Angew. Chem. Int. Ed.* **2016**, *55*, 12538–12542; *Angew. Chem.* **2016**, *128*, 12726–12730.
[32] M. Matsui, K. Takahashi, K. Sakamoto, A. Hirano, Y. Takeda, O. Yamamoto, N. Imanishi, *Dalton Trans.* **2014**, *43*, 1019–1024.

[33] J. Zheng, H. Dang, X. Feng, P.-H. Chien, Y.-Y. Hu, *J. Mater. Chem. A* **2017**, *5*, 18457 – 18463.
[34] M. Rawlence, I. Garbayo, S. Buecheler, J. L. M. Rupp, *Nanoscale* **2016**, *8*, 14746 – 14753.
[35] F. Croce, G. B. Appetecchi, L. Persi, B. Scrosati, *Nature* **1998**, *394*, 456 – 458.
[36] C. Sun, J. Liu, Y. Gong, D. P. Wilkinson, J. Zhang, *Nano Energy* **2017**, *33*, 363 – 386.
[37] M. Rosso, C. Brissot, A. Teyssot, M. Dollé, L. Sannier, J.-M. Tarascon, R. Bouchet, S. Lascaud, *Electrochim. Acta* **2006**, *51*, 5334 – 5340.
[38] J. Rolland, J. Brassinne, J.-P. Bourgeois, E. Poggi, A. Vlad, J.-F. Gohy, *J. Mater. Chem. A* **2014**, *2*, 11839 – 11846.
[39] C. H. Park, D. W. Kim, J. Prakash, Y. K. Sun, *Solid State Ionics* **2003**, *159*, 111 – 119.
[40] Q. Zhang, S.-Z. Huang, J. Jin, J. Liu, Y. Li, H.-E. Wang, L.-H. Chen, B.-J. Wang, B.-L. Su, *Sci. Rep.* **2016**, *6*, 25942.
[41] Z. Lin, X. Guo, H. Yu, *Nano Energy* **2017**, *41*, 646 – 653.
[42] G. Tan, F. Wu, C. Zhan, J. Wang, D. Mu, J. Lu, K. Amine, *Nano Lett.* **2016**, *16*, 1960 – 1968.
[43] F. Wu, N. Chen, R. Chen, Q. Zhu, J. Qian, L. Li, *Chem. Mater.* **2016**, *28*, 848 – 856.
[44] D. Zhou, R. Liu, Y.-B. He, F. Li, M. Liu, B. Li, Q.-H. Yang, Q. Cai, F. Kang, *Adv. Energy Mater.* **2016**, *6*, 1502214.
[45] H. Duan, Y.-X. Yin, X.-X. Zeng, J.-Y. Li, J.-L. Shi, Y. Shi, R. Wen, Y.-G. Guo, L.-J. Wan, *Energy Storage Mater.* **2018**, *10*, 85 – 91.
[46] L. Yang, Z. Wang, Y. Feng, R. Tan, Y. Zuo, R. Gao, Y. Zhao, L. Han, Z. Wang, F. Pan, *Adv. Energy Mater.* **2017**, *7*, 1701437.
[47] Y. Ma, L. B. Li, G. X. Gao, X. Y. Yang, Y. You, *Electrochim. Acta* **2016**, *187*, 535 – 542.
[48] Z. Zhu, M. Hong, D. Guo, J. Shi, Z. Tao, J. Chen, *J. Am. Chem. Soc.* **2014**, *136*, 16461 – 16464.
[49] K. Kimura, M. Yajima, Y. Tominaga, *Electrochem. Commun.* **2016**, *66*, 46 – 48.
[50] R. Tan, R. Gao, Y. Zhao, M. Zhang, J. Xu, J. Yang, F. Pan, *ACS Appl. Mater. Interfaces* **2016**, *8*, 31273 – 31280.
[51] H. Choi, H. W. Kim, J.-K. Ki, Y. J. Lim, Y. Kim, J.-H. Ahn, *Nano Res.* **2017**, *10*, 3092 – 3102.
[52] J. R. Nair, D. Cíntora-Juárez, C. Pérez-Vicente, J. L. Tirado, S. Ahmad, C. Gerbaldi, *Electrochim. Acta* **2016**, *199*, 172 – 179.
[53] W. He, Z. Cui, X. Liu, Y. Cui, J. Chai, X. Zhou, Z. Liu, G. Cui, *Electrochim. Acta* **2017**, *225*, 151 – 159.
[54] C. Tao, M.-H. Gao, B.-H. Yin, B. Li, Y.-P. Huang, G. Xu, J.-J. Bao, *Electrochim. Acta* **2017**, *257*, 31 – 39.
[55] D. Zhou, Y. He, R. Liu, M. Liu, H. Du, B. Li, Q. Cai, Q.-H. Yang, F. Kang, *Adv. Energy Mater.* **2015**, *5*, 1500353.
[56] K. Hayamizu, Y. Aihara, *Solid State Ionics* **2013**, *238*, 7 – 14.
[57] W. Zhou, S. Wang, Y. Li, S. Xin, A. Manthiram, J. B. Goodenough, *J. Am. Chem. Soc.* **2016**, *138*, 9385 – 9388.
[58] C.-Z. Zhao, X.-Q. Zhang, X.-B. Cheng, R. Zhang, R. Xu, P.-Y. Chen, H.-J. Peng, J.-Q. Huang, Q. Zhang, *Proc. Natl. Acad. Sci. USA* **2017**, *114*, 11069 – 11074.
[59] F. Langer, I. Bardenhagen, J. Glenneberg, R. Kun, *Solid State Ionics* **2016**, *291*, 8 – 13.
[60] R. Murugan, V. Thangadurai, W. Weppner, *Angew. Chem. Int. Ed.* **2007**, *46*, 7778 – 7781; *Angew. Chem.* **2007**, *119*, 7925 – 7928.
[61] W. Hua, W. Liu, M. Chen, S. Indris, Z. Zheng, X. Guo, M. Bruns, T.-H. Wu, Y. Chen, B. Zhong, S. Chou, Y.-M. Kang, H. Ehrenberg, *Electrochim. Acta* **2017**, *232*, 123 – 131.

Manuscript received: June 13, 2019
Revised manuscript received: July 31, 2019
Accepted manuscript online: August 6, 2019
Version of record online: September 24, 2019

